Multiple phases with a tricritical point and a Lifshitz point in the skyrmion host Cu_2OSeO_3

Harish Chandr Chauhan, Birendra Kumar, Jeetendra Kumar Tiwari, and Subhasis Ghosh
School of Physical Sciences, Jawaharlal Nehru University, New Delhi 110067, India

(Received 9 April 2019; published 28 October 2019)

Magnetic skyrmions, topologically stable spin swirling objects, have attracted a great interest due to their potential applications in future spintronics and ultrahigh dense magnetic memory devices. Existence of a skyrmion phase as well as first- and second-order phase transitions make Cu_2OSeO_3 a promising candidate for investigating complex magnetic phenomena. Here, we report that both first- and second-order magnetic phase transitions are responsible in determining the phase diagram with at least two multicritical points in Cu_2OSeO_3. A fluctuation-induced first-order transition is realized as a precursor for the skyrmion phase over a small window of temperature and magnetic field. The evolution of isothermal entropy at the phase transition provides evidence for a tricritical point. Furthermore, the existence of commensurate and incommensurate phases along with the coexistence of three second-order phase transitions provide evidence for the existence of a Lifshitz point.

DOI: 10.1103/PhysRevB.100.165143

I. INTRODUCTION

Skyrmions, topologically nontrivial spin-swirling objects that can be treated as a particle of nanometer size, have been observed in various materials with different crystal symmetry and interactions [1–17]. These materials have attracted great interest due to their novel properties and potential applications in future spintronics and magnetic memory devices. Different types of skyrmions have been observed in centrosymmetric [11–14] and noncentrosymmetric [1–10] magnetic materials. In centrosymmetric magnetic materials, the competition between uniaxial magnetic anisotropy and magnetic dipole-dipole interaction causes the formation of magnetic bubbles which are topologically equivalent to skyrmions [11]. In noncentrosymmetric magnetic materials with strong spin-orbit coupling (SOC), skyrmion formation occurs due to competition between two types of exchange interactions: (i) $\vec{S}_i \cdot \vec{S}_j$, symmetric exchange interaction, and (ii) $\vec{D}_{ij} \cdot \vec{S}_i \times \vec{S}_j$, antisymmetric Dzyloshinskii-Moria interaction (DMI) [18,19] where $\vec{S}_i$, $\vec{S}_j$ are the spins at the ith and jth sites respectively and $\vec{D}_{ij}$ is the Dzyloshinskii-Moria vector joining ith and jth site. Two types of skyrmions (Néel and block) have been observed in noncentrosymmetric magnetic materials. The Néel skyrmion is observed in polar magnets such as in GaV_4Se_8 [15], GaV_4S_8 [16], and $VOSe_2O_5$ [17] at significantly low temperature (below 20 K), while the Bloch skyrmion is observed in chiral magnets such as MnSi [1,2], FeGe [3–5], $Fe_{1-x}Co_xSi$ [6,7], and Cu_2OSeO_3 [8–10] in a wide temperature range from 29 K in MnSi to near room temperature in FeGe. MnSi, FeGe, and $Fe_{1-x}Co_xSi$ are metallic whereas Cu_2OSeO_3 is insulating in nature. Cu_2OSeO_3 [20–23] has attracted considerable interest because of the possibility of manipulation of the skyrmion phase by applying an external electric field [9].

Cubic Cu_2OSeO_3 crystallizes in the same space group $P2_13$, as MnSi, FeGe, $Fe_{1-x}Co_xSi$, and other $B20$ materials. It has broken inversion symmetry and threefold rotational symmetry along [111]. Seki *et al.* [8] have observed the skyrmion phase in Cu_2OSeO_3 and shown that there are two inequivalent sites of Cu^{2+} ions surrounded by two types of CuO_5 polyhedra, one with square pyramidal and the other with trigonal bipyramidal structure, in the ratio of 3:1. These two sublattices of Cu^{2+} ions are responsible for local ferrimagnetic ordering in Cu_2OSeO_3 below transition temperature (T_c) [20,22,24]. The competition between DMI and exchange interaction stabilizes the ground state of Cu_2OSeO_3 in helical spin texture with fixed handedness (spin chirality) [8,24]. A weak external field overcomes the helical spin textures and orients the spins along the direction of the field. This weak external field results in the formation of conical phase [25] and skyrmion phase below T_c. In the higher field region, exchange interaction dominates over DMI and induces a conical phase into a field polarized phase [8,24]. Several important properties of Cu_2OSeO_3 and the skyrmion phase observed in Cu_2OSeO_3 have been discussed in previous works [8–10,20–24]. Small-angle neutron scattering (SANS) [9] and Lorentz transmission electron microscopy (LTEM) [8,10] results reflect multiple phases in Cu_2OSeO_3 near T_c, however there are several important issues remaining to be resolved to understand the phase transition and associated phase diagram in Cu_2OSeO_3 as follows: (i) Is the phase diagram of all skyrmionic materials generic? (ii) As both first- and second-order phase transition exists in Cu_2OSeO_3, then where is the tricritical point (TCP)? (iii) Is it necessary to have a precursor phase for the transition from the paramagnetic (PM) to helimagnetic phase? (iv) How are the phase boundaries constructed? Resolving these issues is complicated by the fact that the skyrmion phase is thermodynamically stable only in a small pocket of phase space. In order to investigate these issues thoroughly, we have performed high precision magnetic measurements on Cu_2OSeO_3 over a wide range of magnetic field and temperature. From our investigations, we have been able to report (i) the different phases present in Cu_2OSeO_3 near T_c, (ii) the order of phase transitions between different

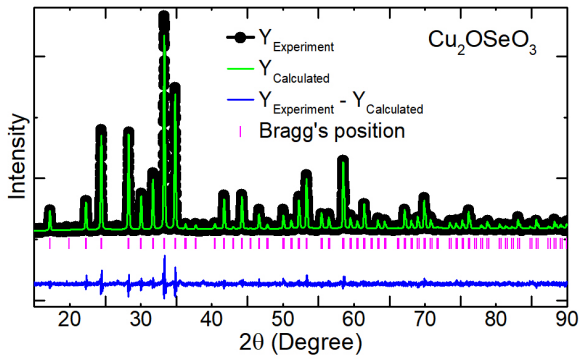

FIG. 1. Reitveld refinement of the XRD data of Cu_2OSeO_3 obtained by Rigaku Miniflex 600 x-ray diffractometer with Cu-K_α radiation. It confirms the formation of single cubic phase of Cu_2OSeO_3 in the space group $P2_13$ with lattice constant $a = b = c = 8.922$ Å and $\alpha = \beta = \gamma = 90^\circ$.

phases, (iii) the existence of a precursor phase required for the transition from the PM to helimagnetic phase, (iv) the existence of TCP and a special multicritical point known as the Lifshitz point (LP), and (v) the almost exact transition lines between phases.

II. EXPERIMENTAL DETAILS

Polycrystalline Cu_2OSeO_3 were grown by the standard solid-state reaction method. A homogeneous mixture of high purity CuO and SeO_2 powder in the molar ratio 2 : 1 was taken. The pellets formed from this mixture were then sealed in an evacuated quartz tube. The quartz ampule was placed horizontally into a muffle furnace and heated to 600 °C with 50 °C/h. We annealed the sample for five weeks by holding the quartz ampule at 600 °C.

X-ray diffraction (XRD). To confirm the cubic phase of Cu_2OSeO_3, we performed powder x-ray diffraction (XRD). The room-temperature XRD data were collected using a Rigaku Miniflex 600 x-ray diffractometer with Cu-K_α radiation. Further, Rietveld refinement using FULLPROF suite software was performed on the XRD data. It confirmed the formation of the single cubic phase of Cu_2OSeO_3 in the space group $P2_13$ with cubic $B20$ structure [26] as shown in Fig. 1.

Magnetic measurements. The magnetic measurements were done using physical properties measurement system (PPMS) by three different methods as follows:

(i) Field cooled (FC) temperature scans: In the presence of a magnetic field, the Cu_2OSeO_3 sample was cooled from room temperature to the desired low temperature. Finally, the temperature-dependent magnetization data were recorded during heating.

(ii) Zero-FC (ZFC) temperature scans: The sample was brought at low temperature and then by applying magnetic field the temperature-dependent magnetization data were recorded during heating.

(iii) ZFC magnetic field scans: The sample was brought at the various required temperatures and held until the thermal equilibrium was reached. First quadrant magnetization (M-H) data were recorded with the step of 1 mT from 0 to 200 mT for exact analysis of phase diagram and associated phase transitions between phases. Above 200 mT the step size was

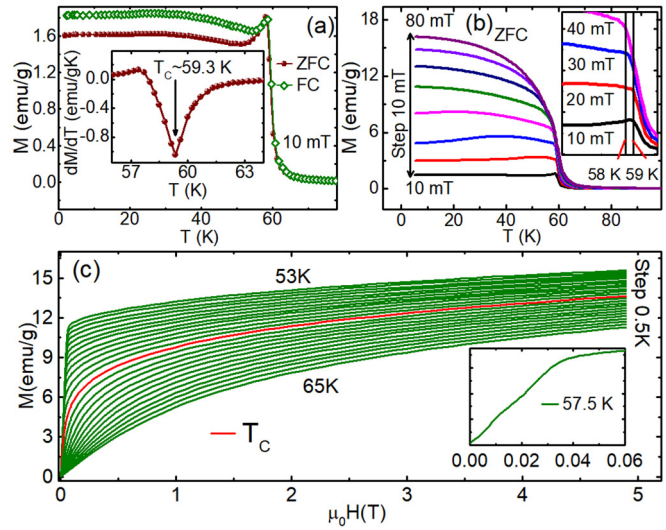

FIG. 2. (a) Field-cooled (FC) and zero-field-cooled (ZFC) data of Cu_2OSeO_3 taken at 10 mT. Inset of (a) is the first derivative of the ZFC data. The minimum gives $T_c = 59.3$ K. (b) ZFC of Cu_2OSeO_3 from 10 to 80 mT with increment step of 10 mT. The variation in the ZFC curves is the clear indication of helimagnetic to field polarized phase transition around 40 mT. The inset shows the magnified view till 40 mT from 50 to 62 K. (c) Field dependent magnetization (M-H) data of Cu_2OSeO_3 at various temperatures from 53 to 65 K with increment step of 0.5 K. No saturation in the M-H data implies nonferromagnetic Cu_2OSeO_3.

increased to 100 mT and data were recorded up to 5 T to analyze the magnetic properties of Cu_2OSeO_3.

III. RESULTS AND DISCUSSION

Field-cooled (FC) and zero-field-cooled (ZFC) curves [Fig. 2(a)] taken at 10 mT show the bifurcation around 59 K. This indicates that the material is paramagnetic above 59 K. The first derivative of the ZFC curve [Fig. 2(a)] gives $T_c = 59.3$ K. The ZFC curves [Fig. 2(b)] show the transition of helimagnetic phase into the field polarized phase above 40 mT. The variation in the ZFC curves is the indication of the existence of multiple phases in Cu_2OSeO_3. Further, we took M-H data up to 5 T at various temperatures ranging from 53 to 65 K with an increment step of 0.5 K as shown in Fig. 2(c). Absence of saturation in the magnetization curves is the clear indication that Cu_2OSeO_3 is nonferromagnetic. The M-H data taken at 57.5 K [inset of Fig. 2(c)] show steplike variation in the magnetic moment. This is again the indication of the existence of multiple phases in Cu_2OSeO_3 below T_c.

A. Arrott plot

The magnetostatic free energy based on Ginzburg's criteria, as a function of the order parameter (magnetization, M) up to M^4, can be reduced to the Arrott relation [27] as

$$M^2 = a\left(\frac{\mu_0 H}{M}\right) + b, \tag{1}$$

where a and b are constants which depend on temperature and magnetic field. Figure 3 shows the Arrott plot of the M-H data

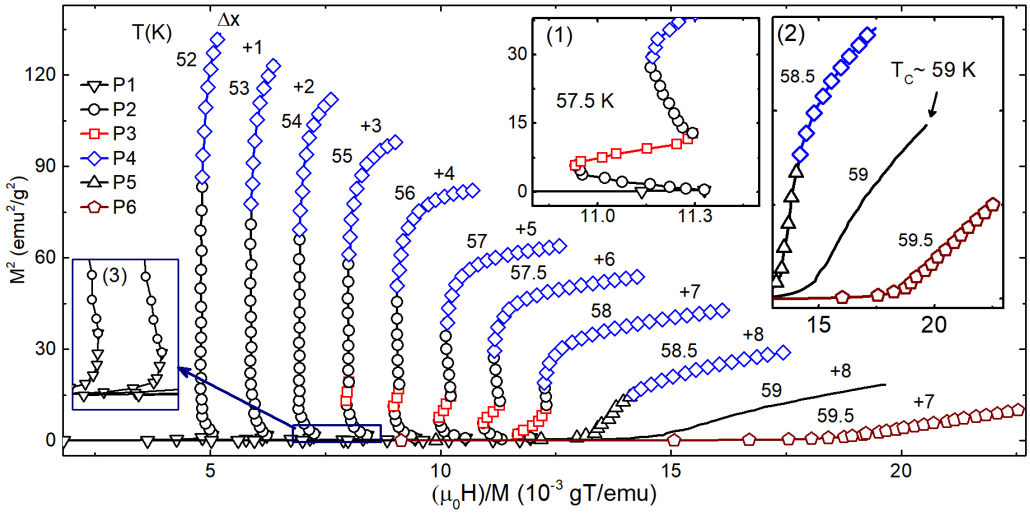

FIG. 3. The Arrott plot of magnetization data up to 60 mT from 52 to 58 K and up to 50 mT above 58 K. The different temperature curves have been moved horizontally to see the clear variation. The different colors represent the phases present in Cu_2OSeO_3. P1 (down triangles): MDH phase; P2 (circles): SDC phase; P3 (squares): skyrmions (*A* phase); P4 (diamonds): field polarized phase; P5 (up triangles) represents the fluctuation disordered phase surrounded by SDC phase, *A* phase, and PM phase; and P6 (pentagons) represents the PM phase. Inset (1) is the Arrott plot at 57.5 K in the field range of 3 to 35 mT. Inset (2) is the magnified view of the Arrott plot at 58.5, 59, and 59.5 K. Inset (3) is the extended view in the vicinity of MDH and SDC phase.

up to 60 mT from 52 to 58 K and up to 50 mT above 58 K. Inset (1) of Fig. 3 shows the Arrott plot at 57.5 K from 3 to 35 mT. It can be seen that there are multiple positive and negative slopes in the Arrott plot below T_c. The change in the slope of the Arrott plot curve is an indication of the field-induced phase transition. The different slope regions in the Arrott plot represent different phases, denoted as P1 (down triangles), P2 (circles), P3 (squares), and P4 (diamonds) corresponding to multidomain helical (MDH) [8], single domain conical (SDC) [1], skyrmion (*A* phase) [1–10], and field polarized phase, respectively. Our result is in agreement with the results obtained from SANS [9,22] and LTEM [8,10]. Inset (2) of Fig. 3 shows the change in the curvature of the Arrott plot from concave to convex [28] around 59 K which is the same as T_c obtained from ZFC [Fig. 2(b)]. The multislope nature of the Arrott curves is vanishing above 58 K, which implies that MDH, SDC, and *A* phase will have the boundary in the vicinity of $T_c' = 58$ K (Fig. 3). The evolution of T_c' is discussed explicitly in a later section of magnetic entropy (Fig. 5). *Hence there must be another phase shown by P5 (up triangles), between T_c' and T_c*. The finite moment [see Fig. 2(c)] in this region confirms the existence of DMI, which is essential as a precursor for the transition from the PM to helimagnetic state. Theoretically, in the case of first-order magnetic transition, it has been shown [29] that the fluctuation induced inhomogeneous phase (with finite moment) is required as a precursor phase for the transition from the PM to helimagnetic state. A similar fluctuation disordered phase may have been observed in MnSi [30]. This phase has been characterized by strongly interacting chiral fluctuation that induces first-order Brazovskii transition [31–33]. Also, according to Banerjee's criteria [34], $a > 0$ in Eq. (1) corresponds to a second-order phase transition and $a < 0$ corresponds to a first-order phase transition at T_c. Thus the transitions from the field polarized to PM and fluctuation disordered to the PM phase are second order.

B. Magnetic entropy

Using Gibbs free-energy expression and Maxwell's relation one can compute the change in entropy, ΔS_M, as

$$\Delta S_M = -\int_{\mu_0 H_1}^{\mu_0 H_2} \left(\frac{\partial M}{\partial T}\right)_{\mu_0 H} d(\mu_0 H). \tag{2}$$

The magnetic entropy change, ΔS_M, in Cu_2OSeO_3 around T_c can be investigated by using the *M-H* data at various temperatures [35]. Figure 4 shows the variation of ΔS_M of Cu_2OSeO_3 with temperature at different applied magnetic fields [Figs. 4(a)–4(i), 5(a), and 5(b)] and with field at different temperatures [Figs. 4(j)–4(r)]. The maximum change in ΔS_M is observed at T_c. The magnitude of change in magnetic entropy increases gradually with applied field. ΔS_M shows a small but clear depth at T_c' [Fig. 5(c)] which changes its position continuously from 58.07 K at 5 mT to 57.5 K at 33 mT [Fig. 5(d)]. This feature, which is absent in all previous work [8–10,23–25], has been observed between T_c' and T_c, and may be of similar origin behind the fluctuation disordered regime reported in [30]. The magnitude of the depth at T_c' first decreases up to 11 mT then increases from 11 to 16 mT and again decreases from 16 to 23 mT. Above 23 mT, the depth at T_c' starts increasing and vanishes near 33 mT [Fig. 5(c)]. It is observed [Figs. 4(a)–4(e)] that ΔS_M starts decreasing when it approaches T_c' and then increases discontinuously above T_c'. This sudden change in ΔS_M implies that the system undergoes a first-order phase transition at T_c' [36]. The variation in ΔS_M is quite fast around T_c until 15 mT [Figs. 4(a) and 4(b)] and continuous above 15 mT [Figs. 4(c)–4(i)] leading to a second-order phase transition [36]. This will violate Bannerjee's

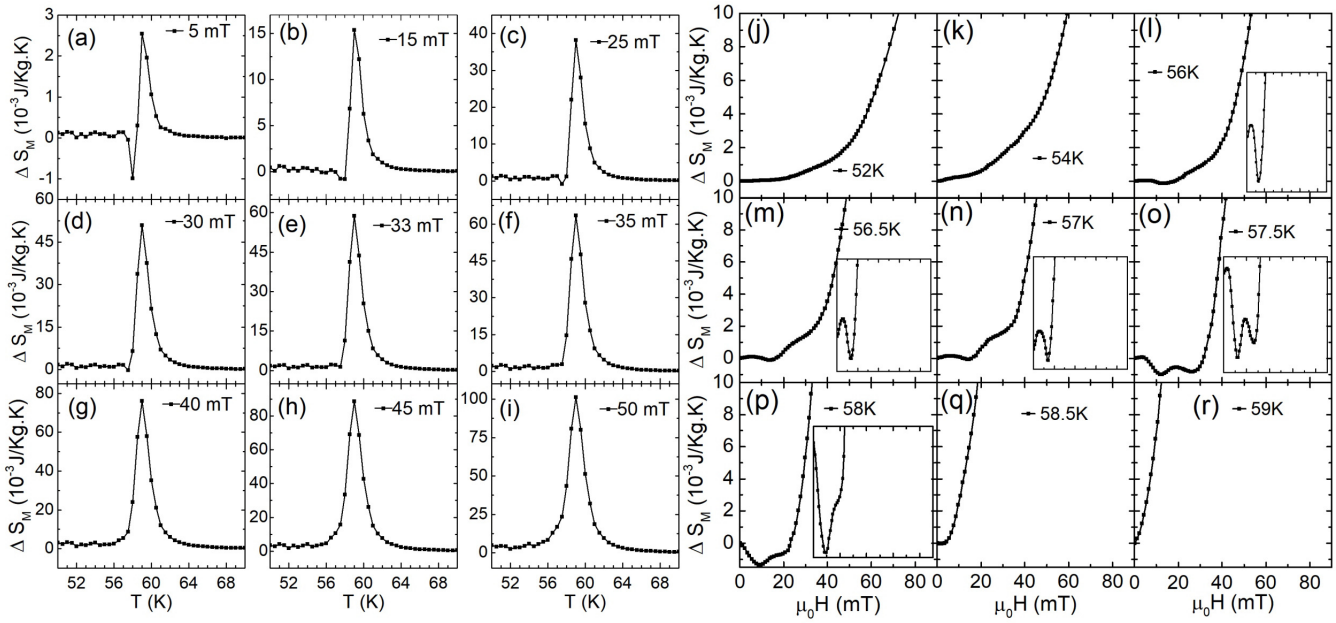

FIG. 4. (a)–(i) Change in entropy, ΔS_M as a function of temperature at different applied magnetic fields varying from 5 to 50 mT. The position of the peak observed near 58.07 K at 5 mT (a) changes with the applied field and disappears at 57.5 K at 33 mT (e). A discontinuous change in slopes of transition curves of ΔS_M is observed around 59 K [(a) and (b)] below 15 mT. This could be due to insufficient data points. The change in entropy, ΔS_M, follows a continuous change in transition curves around 59 K in ΔS_M [(c)–(i)] above 15 mT. (j)–(r) Variation of ΔS_M as a function of applied field at different temperatures. The insets of the graphs are the magnified view near the transition field.

criteria if the transition is first order below 15 mT. Thus the sharp change could be due to insufficient data points near T_c or due to the effect of first-order transition at T_c' because T_c is nearly 1 K away from T_c'.

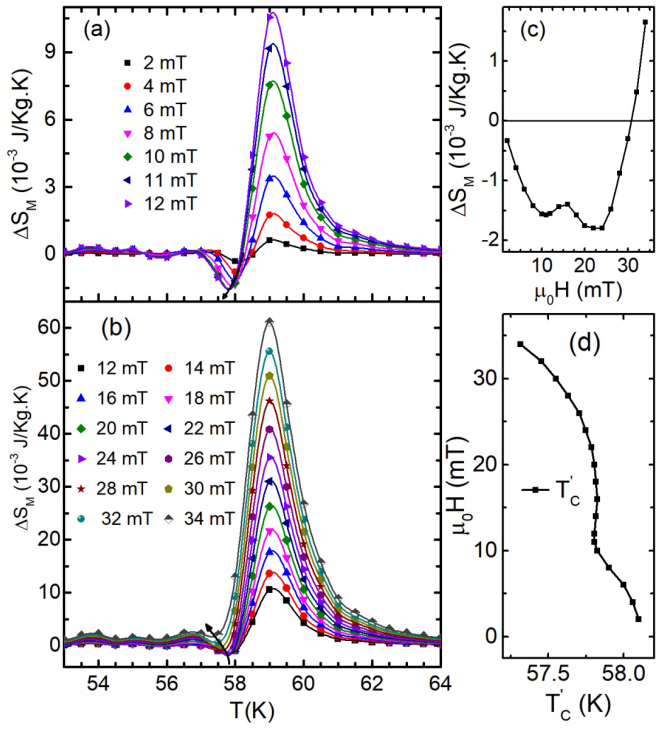

FIG. 5. (a), (b) Spline fit (solid lines) to the ΔS_M curves at different fields. It is found that the variation of the magnitude of ΔS_M varies as shown in (c) which crosses zero near 32 mT and T_c' varies as shown in (d).

A small but significant discontinuous change in ΔS_M has been observed at the transition from the SDC to the A phase [inset of Figs. 4(l)–4(p)]. The change in entropy from the A phase to the SDC phase at the upper boundary is not observed clearly. Since there are only two phases (SDC and fluctuation disordered regime) encompassing the A phase, the transition from the A phase to the SDC phase will be a weak first-order transition [30]. It was observed [Figs. 4(j)–4(o)] that variation of ΔS_M is continuous from MDH to SDC and from SDC to field polarized phases and these are the confirmation for second-order phase transitions. Figure 4(o) shows the discontinuous transition from the A phase to the SDC phase. This is again the evidence of a first-order phase transition from the A phase to the SDC phase (dip near 12 mT) and from the SDC to the fluctuation disordered regime (dip near 28 mT). The feature of change in entropy is observable up to 58 K [Fig. 4(q)]. At 59 K, the change in entropy is maximum; after that it starts decreasing. The smooth variation of ΔS_M (between 58 to 59 K) is again the evidence for the existence of a fluctuation disordered regime between T_c' and T_c.

C. Phase diagram

The phase diagram (Fig. 6) of Cu_2OSeO_3, with all possible phases, have been constructed from the temperature- and field-dependent susceptibility data (Fig. 8). We defined the phase boundaries using various techniques such as (i) Arrott analysis (Fig. 3) to draw the MDH to SDC and SDC to A-phase boundaries, (ii) the change in entropy analysis (Fig. 5) to draw T_c' connecting the MDH, SDC, and A phase to the fluctuation disordered regime, (iii) first derivative of

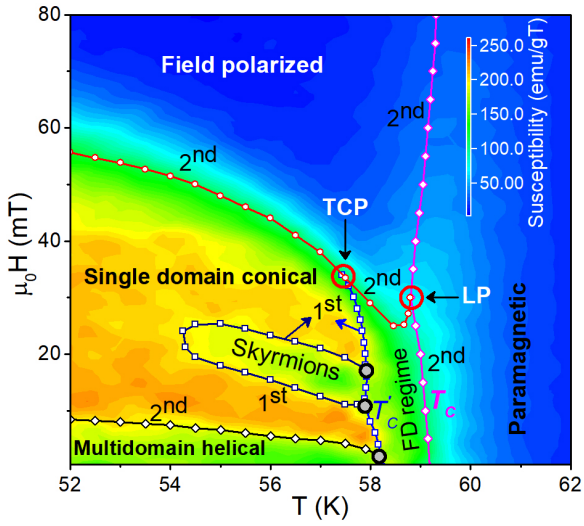

FIG. 6. The magnetic phase diagram of Cu_2OSeO_3 derived from the Arrott plot and entropy analysis. Below T_c, multidomain helical, single domain conical, skyrmion (*A* phase), and field polarized phase are observed. Fluctuation disordered (FD) phase is just below T_c in the width of around 1 K which vanishes at 57.5 K near 33 mT. Paramagnetic phase is above T_c. A tricritical point (TCP) at (57.5 K, 33 mT) and Lifshitz point (LP) at (58.8 K, 30 mT) are observed. All the orders of phase transitions are mentioned in the figure.

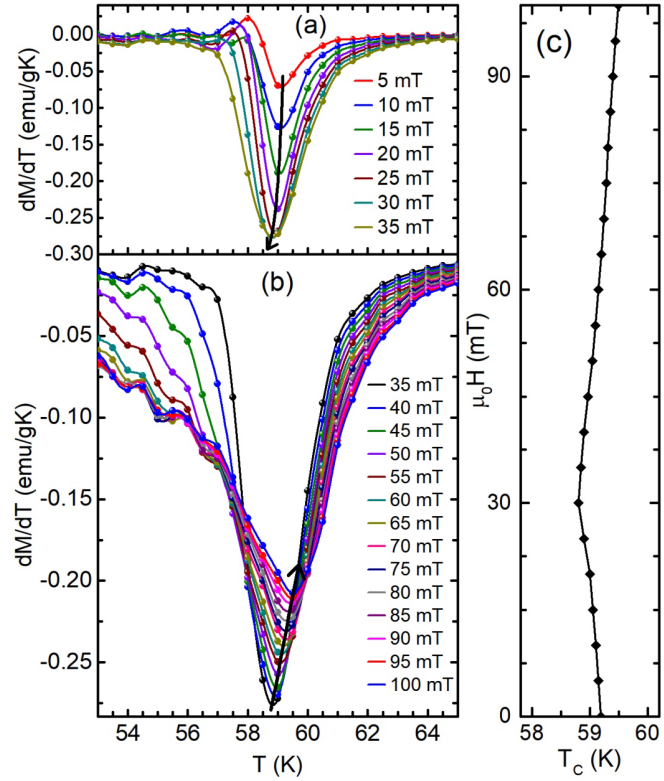

FIG. 7. The transition line connecting the PM phase to other phases from 0 to 100 mT is the line joining the transition temperatures (T_c's) obtained at different fields. The first derivative of ZFC gives T_c's at different fields as shown in (a) and (b) in the form of solid spheres. We did the spline fit (solid lines) to the curves to reduce the error in the measurement of T_c. The transition line connecting the value of T_c's at different fields is shown in (c).

the temperature-dependent magnetization data were taken at various magnetic fields [Fig. 2(c)] to draw field-dependent T_c (Fig. 7) connecting the fluctuation disordered regime and field polarized phase to the PM phase, and (iv) scaling of the susceptibility curves (Fig. 8) obtained from the *M*-*H* curves [Fig. 2(c)] to construct the boundary of the field polarized phase connecting the SDC, PM phase, and fluctuation disordered regime. After analyzing the phase diagram, one can obtain the transition line connecting the field polarized phase with the fluctuation disordered regime and SDC phase by differentiating the susceptibility curves (Fig. 8). We have tried a different technique to obtain the transition line. It has been observed that the first derivative of the ZFC plot [Fig. 2(a)] gives the transition temperature T_c. The value of T_c obtained is the point of inflection on the ZFC curve. So, we have scaled the susceptibility curves (Fig. 8) in such a way that the value of susceptibility near the transition lines becomes the same for all curves. Thus, the color contour of the constructed phase diagram using the scaled susceptibility data represents a single color transition line from field polarized to other phases. With the help of the transition line from the PM to field polarized phase [Fig. 7(c)], the transition line connecting the field polarized to other phases has been constructed as shown in Fig. 9. The variation of the transition line T_c gives an indication that two different phases (which are fluctuation disordered regime and field polarized phase) meet near 30 mT at $\simeq$58.8 K.

The transition lines connecting phases are shown in the phase diagram (Fig. 6). As seen clearly, the first-order transition line T_c' becomes second order at (57.5 K, 33 mT) where the SDC, fluctuation disordered regime, and field polarized phases meet. These observations suggest that (57.5 K, 33 mT) must be a TCP [30]. Further, the colinear spins are responsible for the field polarized phase to be commensurate while noncolinear spins make the helimagnetic phase an incommensurate phase [37]. The presence of antisymmetric

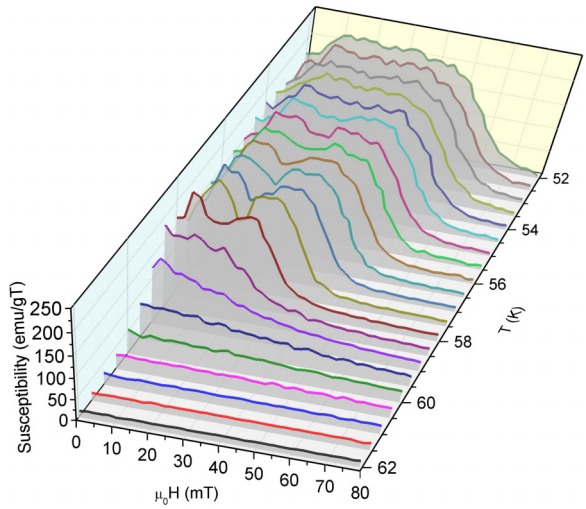

FIG. 8. The plot of magnetic susceptibility data obtained from the derivative of the *M*-*H* data taken at various temperatures.

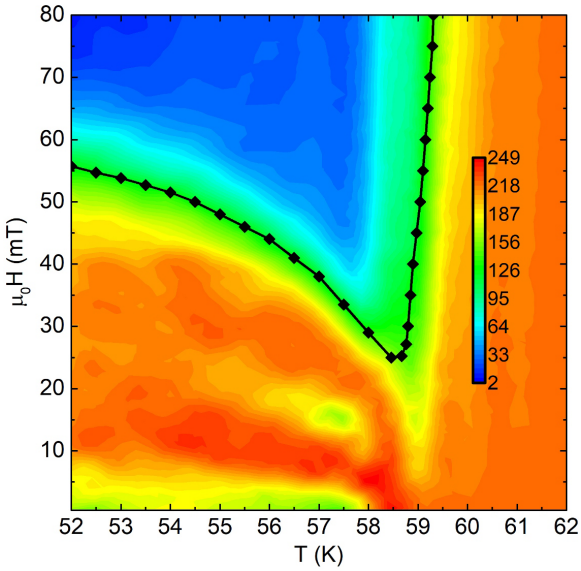

FIG. 9. The color contour of the constructed phase diagram using the scaled susceptibility data represents a single color transition line from field polarized phase to other phases. Taking the help of the transition line (T_c) from PM to field polarized phase as shown in Fig. 7(c), the transition line connecting field polarized to other phases has been constructed as shown.

DMI is responsible for the fluctuation disordered regime to be an incommensurate phase [38]. Also, the field polarized, fluctuation disordered regime and the PM phase are observed to meet tangentially at (58.8 K, 30 mT). Based on these observations, the point (58.8 K, 30 mT) can be interpreted as a Lifshitz point (LP) which was proposed by Honreich, Luban, and Shtrikman [39] as a special multicritical point with an incommensurate phase joining all three phases with a common tangent. Similar LPs have been observed in UPd_2Si_2 [37], $UAs_{1-x}Se_x$ [40], $LaCrGe_3$ [41], and a variety of different systems [37,38,42,43]. The LP provides a clear insight into how three phases, out of which one must be an incommensurate phase, evolve in the system. The LP confirms that the fluctuation disordered phase is the incommensurate phase in Cu_2OSeO_3. These multicritical points also indicate the existence of multiple phases in a material.

IV. CONCLUSION

In conclusion, we have presented a comprehensive study on the phase diagram and the order of phase transition between phases near T_c in multiferroic Cu_2OSeO_3. The existence of two unequal sublattices and nonsaturating M-H curves confirm ground-state local ferrimagnetic ordering in Cu_2OSeO_3. The detailed study of the Arrott plot is done in the region where multiple phases have been reported in Cu_2OSeO_3. Different slope regions observed in the Arrott plot are investigated to represent different phases in Cu_2OSeO_3. The skyrmion phase is determined in a small pocket of applied field and temperature. The transition temperature estimated from the Arrott plot matches very well with the T_c calculated from the ZFC curve. A small but significant positive slope region is observed just below T_c in the Arrott plot, which is concluded as the precursor phase, known as the fluctuation disordered regime. This precursor phase is required for the formation of the skyrmion phase. We have also investigated the second-order phase transition from the precursor and field polarized phase to the PM phase. Further, the order of phase transition and the existence of multiple phases are estimated from the change in magnetic entropy analysis. Again, an apparent anomaly of the fluctuation disordered regime is observed just below T_c, which ends around ($\sim$57.5 K, $\sim$33 mT). The first-order phase transition has been estimated to the transition lines connecting the fluctuation disordered regime to the helimagnetic phase and the skyrmion (A phase) to the SDC phase. The rest of the transition lines are observed to exhibit a second-order phase transition.

Finally, the phase diagram of Cu_2OSeO_3 has been constructed near T_c from isothermal susceptibility data. The multiple phases, transition lines, and the order of phase transition among the phases have been estimated from various techniques as discussed above. A TCP has been observed at (57.5 K, 33 mT) where the first-order transition line (the fluctuation disordered regime to the helimagnetic phase) changes to second order (the SDC to the field polarized phase). A closer analysis of the phase diagram confirms the existence of the Lifshitz point at (58.8 K, 30 mT). Also, first-order transition lines joining the SDC, skyrmion, and fluctuation disordered regime are meeting at two singular points which could represent a triple point in the system. Three phases, viz. the MDH, SDC, and fluctuation disordered regime, are meeting at a singular point which is still inconclusive. In spite of the insulating helimagnetic nature of Cu_2OSeO_3, it is concluded that the presented phase diagram could be generic for all $B20$ compounds possessing the skyrmion phase. Other skyrmionic $B20$ materials are needed to review to confirm the robustness of our analysis.

ACKNOWLEDGMENTS

We thank AIRF-JNU for providing facilities for PPMS and XRD measurement. H.C.C. acknowledges UGC-CSIR, India for financial support through a fellowship. This project was partially supported by DST-PURSE, Government of India.

[1] S. Mühlbauer, B. Binz, F. Jonietz, C. Pfleiderer, A. Rosch, A. Neubauer, R. Georgii, and P. Böni, Science **323**, 915 (2009).

[2] A. Tonomura, X. Yu, K. Yanagisawa, T. Matsuda, Y. Onose, N. Kanazawa, H. S. Park, and Y. Tokura, Nano Lett. **12**, 1673 (2012).

[3] H. Wilhelm, M. Baenitz, M. Schmidt, U. K. Rößler, A. A. Leonov, and A. N. Bogdanov, Phys. Rev. Lett. **107**, 127203 (2011).

[4] X. Z. Yu, N. Kanazawa, Y. Onose, K. Kimoto, W. Z. Zhang, S. Ishiwata, Y. Matsui, and Y. Tokura, Nat. Mater. **10**, 106 (2011).

[5] E. Moskvin, S. Grigoriev, V. Dyadkin, H. Eckerlebe, M. Baenitz, M. Schmidt, and H. Wilhelm, Phys. Rev. Lett. **110**, 077207 (2013).

[6] W. Münzer, A. Neubauer, T. Adams, S. Mühlbauer, C. Franz, F. Jonietz, R. Georgii, P. Böni, B. Pedersen, M. Schmidt, A. Rosch, and C. Pfleiderer, Phys. Rev. B **81**, 041203(R) (2010).

[7] H. S. Park, X. Yu, S. Aizawa, T. Tanigaki, T. Akashi, Y. Takahashi, T. Matsuda, N. Kanazawa, Y. Onose, D. Shindo, A. Tonomura, and Y. Tokura, Nat. Nanotechnol. **9**, 337 (2014).

[8] S. Seki, X. Z. Yu, S. Ishiwata, and Y. Tokura, Science **336**, 198 (2012).

[9] S. Seki, J. H. Kim, D. S. Inosov, R. Georgii, B. Keimer, S. Ishiwata, and Y. Tokura, Phys. Rev. B **85**, 220406(R) (2012).

[10] T. Lancaster, R. C. Williams, I. O. Thomas, F. Xiao, F. L. Pratt, S. J. Blundell, J. C. Loudon, T. Hesjedal, S. J. Clark, P. D. Hatton, M. Ciomaga-Hatnean, D. S. Keeble, and G. Balakrishnan, Phys. Rev. B **91**, 224408 (2015).

[11] X. Yu, Y. Tokunaga, Y. Kaneko, W. Zhang, K. Kimoto, Y. Matsui, Y. Taguchi, and Y. Tokura, Nat. Commun. **5**, 3198 (2014).

[12] A. Kotani, H. Nakajima, K. Harada, Y. Ishii, and S. Mori, Phys. Rev. B **95**, 144403 (2017).

[13] X. Yu, Y. Tokunaga, Y. Taguchi, and Y. Tokura, Adv. Mater. **29**, 1603958 (2017).

[14] X. Yu, M. Mostovoy, Y. Tokunaga, W. Zhang, K. Kimoto, Y. Matsui, Y. Kaneko, N. Nagaosa, and Y. Tokura, Proc. Natl. Acad. Sci. U. S. A **109**, 8856 (2012).

[15] Y. Fujima, N. Abe, Y. Tokunaga, and T. Arima, Phys. Rev. B **95**, 180410(R) (2017).

[16] I. Kézsmárki, S. Bordács, P. Milde, E. Neuber, L. M. Eng, J. S. White, H. M. Rønnow, C. D. Dewhurst, M. Mochizuki, K. Yanai, H. Nakamura, D. Ehlers, V. Tsurkan, and A. Loidl, Nat. Mater. **14**, 1116 (2015).

[17] T. Kurumaji, T. Nakajima, V. Ukleev, A. Feoktystov, T.-h. Arima, K. Kakurai, and Y. Tokura, Phys. Rev. Lett. **119**, 237201 (2017).

[18] I. Dzyaloshinsky, J. Phys. Chem. Solids **4**, 241 (1958).

[19] T. Moriya, Phys. Rev. **120**, 91 (1960).

[20] J.-W. G. Bos, C. V. Colin, and T. T. M. Palstra, Phys. Rev. B **78**, 094416 (2008).

[21] K. H. Miller, X. S. Xu, H. Berger, E. S. Knowles, D. J. Arenas, M. W. Meisel, and D. B. Tanner, Phys. Rev. B **82**, 144107 (2010).

[22] M. Belesi, I. Rousochatzakis, H. C. Wu, H. Berger, I. V. Shvets, F. Mila, and J. P. Ansermet, Phys. Rev. B **82**, 094422 (2010).

[23] E. Ruff, P. Lunkenheimer, A. Loidl, H. Berger, and S. Krohns, Sci. Rep. **5**, 15025 (2015).

[24] T. Adams, A. Chacon, M. Wagner, A. Bauer, G. Brandl, B. Pedersen, H. Berger, P. Lemmens, and C. Pfleiderer, Phys. Rev. Lett. **108**, 237204 (2012).

[25] F. Qian, H. Wilhelm, A. Aqeel, T. T. M. Palstra, A. J. E. Lefering, E. H. Brück, and C. Pappas, Phys. Rev. B **94**, 064418 (2016).

[26] H. Effenberger and F. Pertlik, Monatsch. Chem. **117**, 887 (1986).

[27] A. Arrott, Phys. Rev. **108**, 1394 (1957).

[28] P. Jain, D. Bansal, G. Sharma, A. Bhattacharya, B. Ingale, O. Delaire, and R. CHatterjee, J. Phys. Cond. Matt. **30**, 075801 (2018).

[29] G. J. Conduit, A. G. Green, and B. D. Simons, Phys. Rev. Lett. **103**, 207201 (2009).

[30] A. Bauer, M. Garst, and C. Pfleiderer, Phys. Rev. Lett. **110**, 177207 (2013).

[31] M. Janoschek, M. Garst, A. Bauer, P. Krautscheid, R. Georgii, P. Böni, and C. Pfleiderer, Phys. Rev. B **87**, 134407 (2013).

[32] S. M. Stishov, A. E. Petrova, A. A. Shikov, T. A. Lograsso, E. I. Isaev, B. Johansson, and L. L. Daemen, Phys. Rev. Lett. **105**, 236403 (2010).

[33] F. Krüger, U. Karahasanovic, and A. G. Green, Phys. Rev. Lett. **108**, 067003 (2012).

[34] B. K. Banerjee, Phys. Lett. **12**, 16 (1964).

[35] V. Franco, C. F. Conde, J. S. Blázquez, A. Conde, P. Švec, D. Janičkovič, and L. F. Kiss, J. Appl. Phys. **101**, 093903 (2007).

[36] A. Fujita, S. Fujieda, K. Fukamichi, Y. Yamazaki, and Y. Ijima, Mater. Trans. **43**, 1202 (2002).

[37] T. Plackowski, D. Kaczorowski, and J. Sznajd, Phys. Rev. B **83**, 174443 (2011).

[38] A. Zheludev, S. Maslov, G. Shirane, Y. Sasago, N. Koide, and K. Uchinokura, Phys. Rev. Lett. **78**, 4857 (1997).

[39] R. M. Hornreich, M. Luban, and S. Shtrikman, Phys. Rev. Lett. **35**, 1678 (1975).

[40] T. Plackowski, M. Matusiak, and J. Sznajd, Phys. Rev. B **82**, 094408 (2010).

[41] U. S. Kaluarachchi, S. L. Bud'ko, P. C. Canfield, and V. Taufour, Nat. Commun. **8**, 546 (2017).

[42] R. M. Hornreich, J. Magn. Magn. Mater. **15-18**, 387 (1980).

[43] S. L. Qiu, M. Dutta, H. Z. Cummins, J. P. Wicksted, and S. M. Shapiro, Phys. Rev. B **34**, 7901 (1986).